Chemical Papers (2022) 76:6223–6233
https://doi.org/10.1007/s11696-022-02311-z

ORIGINAL PAPER

In situ green synthesis of cellulose nanocomposite films incorporated with silver/silver chloride particles: characterization and antibacterial performance

Mozhgan Bagheri[1] · Mojgan Heydari[1] · Parvaneh Sangpour[1] · Sasan Rabieh[2]

Received: 11 February 2022 / Accepted: 31 May 2022 / Published online: 18 June 2022

Abstract

Ag/AgCl@cellulose nanocomposite films were fabricated based on microwave-assisted ionic liquid method using 1-butyl-3-methylimidazolium chloride ($[C_4mim]Cl$) with $AgNO_3$. The ionic liquid acted as a solvent for dissolution of cellulose and served as the chlorine source for in situ precipitation of silver chloride in the cellulose matrix. Ag/AgCl was formed within the cellulose matrix due to the partial reduction of AgCl in the cellulose matrix to Ag^0 upon exposure to ambient light in the synthesis process. Optical microscopy, scanning electron microscopy, energy-dispersive X-ray spectroscopy, transmission electron microscopy, Fourier transform infrared, X-ray diffraction, X-ray photoelectron spectroscopy, and thermogravimetric analysis were used to characterize morphology, crystal structure, composition, and thermal stability of Ag/AgCl@cellulose nanocomposites. Morphological evaluation showed the cube-like Ag/AgCl particles anchored on the surface of cellulose and embedded within the interlaced cellulose matrix as well. The composite films have localized surface plasmon resonance at 480 nm, indicating formation of the silver nanoregions on the silver chloride particle surface. The antibacterial potency of the nanocomposite films was assessed against bacterial strains of *E. Coli* and *S. Aureus*. The antibacterial tests showed growth prevention of the two representative strains of Gram-positive and Gram-negative bacteria.

Graphical abstract

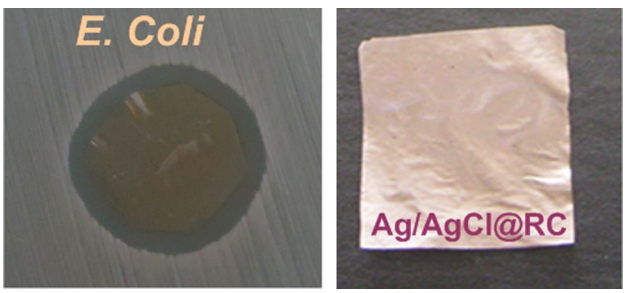

Keywords Cellulose · Ag/AgCl · Nanocomposite · Ionic liquid · Antibacterial

Introduction

The resistance of pathogens to conventional antibiotics is a public health issue which needs to be overcome in an effective way (Abdelhameed et al. 2018, 2019; Darwesh et al. 2019). Silver-based antimicrobials can be used as promising alternatives to solve antimicrobial resistance problems. Silver-based materials have been widely used as antimicrobial agents in the healthcare and food industry.

✉ Mozhgan Bagheri
m.bagheri@merc.ac.ir

[1] Nanotechnology and Advanced Materials Department, Materials and Energy Research Center, Karaj, Iran

[2] Department of Molecular Pathobiology, Division of Biomaterials, New York University College of Dentistry, New York, NY 10010, USA

Polymer-supported silver-based nanostructures have been used in various biomedical applications, such as wound dressing materials, body wall repairs, tissue scaffolds, and antimicrobial filters (Sarac 2016). For these applications, it is necessary to support silver nanostructures in a biocompatible polymer (Rehan et al. 2020; Abdel-Monem et al. 2020; Vosmanská et al. 2015). Polysaccharides are popular polymeric supports for nanoparticles since they are highly stable, non-toxic, hydrophilic, and biodegradable materials that can be easily chemically modified (Alavi and Rai 2019). Cellulose is a biocompatible and biodegradable polysaccharide consisting of linear chains of D-glucose units (Franz and Blaschek 1990; Kontturi et al. 2006; Stevanovic 2018). Cellulose has a highly ordered crystalline structure due to inter- and intra-hydrogen bonding between chains (Qi 2017). The high crystallinity and the hydrogen bonds in the cellulose structure make it insoluble in water and in the most conventional organic solvents as well.

Ionic liquids are a group of organic salts which are liquid at a relatively low temperature (100 °C). They are thermally and chemically stable, non-flammable, and have low vapor pressure. Ionic liquids have been used in various chemical reactions and processes (Vekariya 2017). They have also been used as a green solvent for cellulose regeneration (Silva et al. 2015; Zhang et al. 2017; Sayyed et al. 2019; Koide et al. 2019; Verma et al. 2019). 1-Butyl-3-methylimidazolium chloride ($[C_4mim]Cl$) is an effective ionic liquid solvent which can solubilize cellulose through breaking down the intra- and inter-molecular interactions in the cellulose structure (Swatloski et al. 2002; Liu et al. 2015).

There are a number of reports on the fabrication of cellulose–silver nanocomposites (Stejskal et al. 2008; Kucekova et al. 2013; Alavi and Rai 2019; Kumar et al. 2018; Islam et al. 2019; Gudimalla et al. 2022), with cotton fiber as cellulose source for immobilization of silver nanoparticles (Ahmed et al. 2020; Katouah and El-Metwaly 2021; Atta 2021; Atta and Abomelka 2021; El-Naggar et al. 2021) and cellulose-AgX nanocomposites (Dong et al. 2013; Vosmanská et al. 2015; Wang et al. 2017; Ma et al. 2018; Lal and Mhaske 2018). However, the reports on the fabrication of nanocomposites of cellulose-Ag/AgCl cellulose are limited. Liu et al. (2012) reported the fabrication of bacterial cellulose-Ag/AgCl nanocomposite as an antibacterial material by the bacterium *Gluconacetobacter xylinus*. Dai et al. (2017) and Dong et al. (2014) obtained hybrids of Ag/AgCl with cellulose based on the effect of the chemical and physical properties of ultrasound agitation. Wang et al. (2016) fabricated cellulose-Ag@AgCl composites as a photocatalyst by electrospinning the solution of cellulose, LiCl, and dimethylacetamide with silver nitrate under visible light. Zhou et al. (2016) applied electrospun cellulose acetate membrane as a support for Ag@AgCl crystals.

Peng et al. (2017) prepared cellulose-Ag@AgCl composite films as an effective photocatalyst through coagulation of cellulose and 1-butyl-3-methylimidazolium chloride solution with silver nitrate and polyvinyl pyrrolidone. Shu et al. (2018) synthesized the cellulose-Ag@AgCl composites through one-step coagulation using cotton as cellulose source and investigated anti-fouling properties of the composite. Ag@AgCl cellulose hydrogel was synthesized by Tang et al. (2018) in which chlorine was supplied by cellulose cross-linker. Zhang et al. (2018) reported preparation of cellulose-Ag@AgCl composite as an antibacterial film by coagulation of the solution of cellulose, LiCl, and dimethylacetamide with silver nitrate and polyvinyl pyrrolidone.

In one of the previous studies, Dong et al. (2013) used microwave-assisted ionic liquid method using different ionic liquids and ascorbic acid as the reducing agent for synthesis of cellulose-AgX/Ag hybrids (X = Br and Cl). They observed AgCl crystals did not grow in a cellulose matrix in the applied conditions. In comparison, in our study, we successfully synthesized the Ag/AgCl@cellulose nanocomposites in situ using microwave-assisted ionic liquid method. In this work, the ionic liquid $[C_4mim]Cl$ acted as a solvent for dissolution of cellulose and served as the chlorine source for the synthesis of silver chloride in the cellulose matrix. A fraction of silver ions in silver chloride structure is reduced to Ag^0 under ambient light, and a hybrid of silver/silver chloride is formed. Synthesized Ag/AgCl@cellulose nanocomposites with high content of Ag/AgCl nanoparticles (20 and 40%) act as a good candidate in antimicrobial membranes.

Experimental

Chemicals

1-Butyl chloride, N-methyl imidazole, diethyl ether, and ethanol were obtained from Merck (Germany). $AgNO_3$ and microcrystalline cellulose (MCC, 20-μm powders) were purchased from Sigma-Aldrich.

Preparation of Ag/AgCl@cellulose nanocomposite films

1-Butyl-3-methylimidazolium chloride ($[C_4mim]Cl$) ionic liquid (IL) was synthesized based on the reaction of N-methyl imidazole and 1-buthyl chloride according to our previous work (Bagheri and Rabieh 2013). Synthesized $[C_4mim]Cl$ was used for dissolution of cellulose and preparation of the nanocomposite of Ag/AgCl@cellulose. For this purpose, 0.25 g MCC was dissolved in 5.0 g $[C_4mim]Cl$ using microwave pulse heating (2 min, 3–5 s pulse) and then $AgNO_3$ (0.25 g) was added to the solution and manually mixed and heated further for 1 min. Then, the mixture

was cast as a film on a glass plate using a coating rod. IL solvent was leached from the film using water, and AgCl@cellulose film (a white color film) was formed. AgCl in the cellulose matrix was partially decomposed into Ag^0 under ambient light with reconstruction of Ag/AgCl@cellulose (a violet colored film). The cellulose film was air-dried at room temperature. The regenerated cellulose film which was not treated with silver ions was coded the regenerated cellulose (RC). The Ag/AgCl@cellulose nanocomposite films treated with silver ions with Ag to cellulose ratio of 20 and 40% were coded as Ag/AgCl@RC-20 and Ag/AgCl@RC-40, respectively.

Characterization of the Ag/AgCl@RC films

A high-resolution scanning electron microscope (VEGA/TESCAN) and a Zeiss (EM10C-Germany) transmission electron microscope (TEM) were used for morphological observations. Specimens were coated with gold to make the surface conductive. Fourier transform infrared spectra were carried out using a PerkinElmer FT-IR Spectrometer. Thermal stability of the films was performed using PL-STA-1640 thermal analyzer. The temperature ranged from 25 to 600 °C with a 5 °C min^{-1} heating rate in the air. Diffuse reflectance spectra were collected using Diffuse Reflection Spectrometer (Avaspec-2048-TEC). Surface modification of the films was characterized by X-ray Photoelectron Spectroscopy (Bestec) with monochromatic Al Kα X-rays (1486.6 eV) as photon source.

Study of antimicrobial activity of Ag/AgCl@RC nanocomposite films

Antibacterial activity of the nanocomposites against *E. Coli* (*Escherichia Coli*, Gram-negative bacterium) and *S. Aureus* (*Staphylococcus Aureus*, Gram-positive bacterium) was investigated by disc diffusion and CFU (colony forming count) methods. In the disc diffusion method, agar nutrient was poured into the Petri dish and solidified. *E. Coli* and *S. Aureus* bacteria were then spread over agar plate. Then, the control sample (RC film) and the Ag/AgCl@RC films were cut in circular shape and placed on bacteria-cultured agar plates and incubated at 37 °C for 24 h.

In the CFU method, all the test tubes containing 10 ml of growth medium were seeded with fresh *E. Coli* and *S. Aureus* at a concentration of 1×10^6 colony forming units per ml (CFU/ml). Ag/AgCl@RC films and RC film (control sample) were sliced into small pieces and sterilized. 0.001 g of each finely sliced film was added to a tube and incubated at 37 °C for 12 h in a shaker incubator. After incubation, media were serially diluted (10^2 to 10^5 times). Then, 50 µl of each bacterial suspension was cultured on an agar plate and was incubated at 37 °C for 12 h. Counting of the survived bacterial colonies was performed by an electronic colony counter (Sana SL-902) in triplicates for each trial. The percentage of the antimicrobial activity was calculated using Eq. (1):

$$\text{Antimicrobial activity } \% = (A - B)/A \times 100 \quad (1)$$

where A and B are number of colonies in control plate (RC) and the sample plate (Ag/AgCl@RC), respectively.

Results and discussion

Optical property of the Ag/AgCl@RC

Figure 1 shows optical images of the regenerated cellulose (RC) and Ag/AgCl@RC nanocomposites. The color of cellulose films containing Ag/AgCl is violet, while RC film is transparent with no color. The violet color of Ag/AgCl@RC

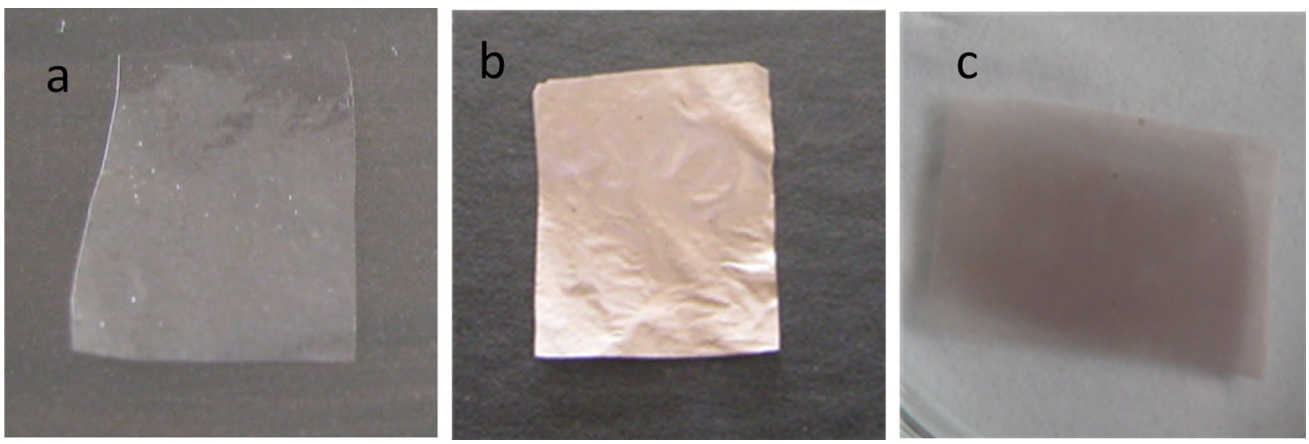

Fig. 1 Optical image of RC film (**a**), Ag/AgCl@RC film at dried (**b**), and wet forms (**c**)

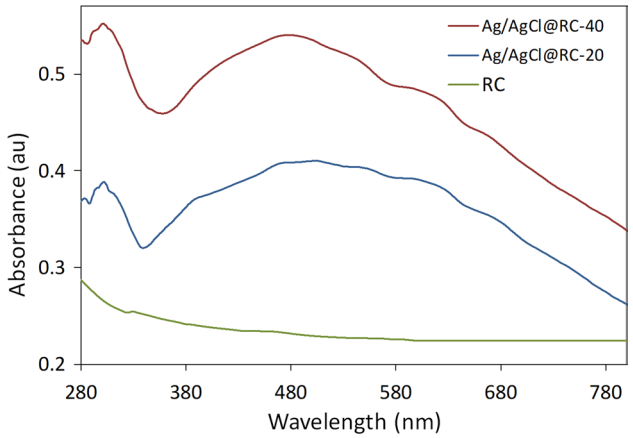

Fig. 2 UV–Vis diffuse reflectance spectra of RC and Ag/AgCl@RC nanocomposite

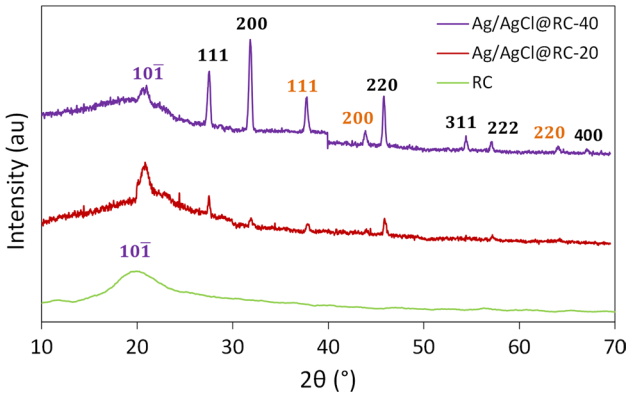

Fig. 3 X-ray diffraction patterns of RC and Ag/AgCl@RC nanocomposite films

is due to the formation of Ag^0 nanodomains on the surface of AgCl. Figure 2 shows the UV–visible diffuse reflectance spectra of the RC and Ag/AgCl@RC nanocomposites. As seen in Fig. 2, no absorbance peak is observed in the spectrum of RC sample, while the nanocomposites have wide visible spectra with λ_{max} of 480 nm. The peaks in the visible light region of the nanocomposite films are assigned to the surface plasmon resonance of the silver nanoregions on the surface of silver chloride particles (Choi et al. 2010; Song et al. 2013; Cheng et al. 2015; Trinh et al. 2015; Alahmadi et al. 2018; Dong et al. 2012). Partially reducing silver ions in silver chloride to silver nanoparticles within the cellulose matrix is induced by ambient light in the synthesis process (Chen et al. 2014).

Also the peaks observed at ultraviolet region of the Ag/AgCl@RC nanocomposites (λ of 302 nm) are absorbance characteristic of AgCl particles, which has a direct band gap of 5.6 eV and an indirect band gap of 3.25 eV (Trinh et al. 2015; Kumar et al. 2016; Zhao et al. 2015). The obtained results are in agreement with the violet color of the Ag/AgCl@RC nanocomposite films due to the presence of silver nanodomains in the structure of nanocomposite.

X-ray diffraction of the Ag/AgCl@RC nanocomposite

The phases and crystalline structure of the films were studied by X-ray diffraction. Figure 3 shows the XRD patterns of the RC and Ag/AgCl@RC nanocomposite. The XRD pattern of RC film shows a reflection at 2θ value of 20.5 attributed to the 10$\bar{1}$ crystal lattice of cellulose II (Langan et al. 2005). This reflection shows conversion of the crystalline structure of cellulose I to cellulose II due to its dissolution in ionic liquid and regeneration as a film. This reflection is also observed in Ag/AgCl@RC films, which means the presence of Ag/AgCl did not alter the crystal structure of the cellulose matrix in the nanocomposite films. The other peaks observed in XRD pattern of Ag/AgCl@RC nanocomposites at 2θ value of 38.1, 44.3, and 64.4 are assigned to the reflections of the (111), (200), and (220) of cubic metallic Ag, respectively (card no of 00–004-0783). The residual peaks at 2θ value 27.8, 32.3, 46.3, 54.9, 57.5, and 67.4 are related to (111), (200), (220), (311), (222), and (400) crystal planes of the silver chloride cubic structure, respectively (card no of 00-001-1013) (Liu et al. 2012). No peaks of silver nitrate were observed in the XRD pattern of nanocomposite indicating Ag/AgCl@RC films achieved without any impurities.

Figure 3 shows AgCl is the major phase and Ag nanoparticles have lower intensity than that of AgCl. Silver chloride in the cellulose matrix was formed due to the chemical reaction between silver ions and the chloride anion of 1-butyl-3-methyl chloride. The fraction of silver in the AgCl lattice was converted into Ag nanoparticles under ambient light exposure during the Ag/AgCl@RC synthesis process. Therefore, no complete transformation of AgCl into Ag nanoparticles in the nanocomposites occurred during the reduction process under ambient light. XRD results were in good agreement with visible spectra and confirm the formation

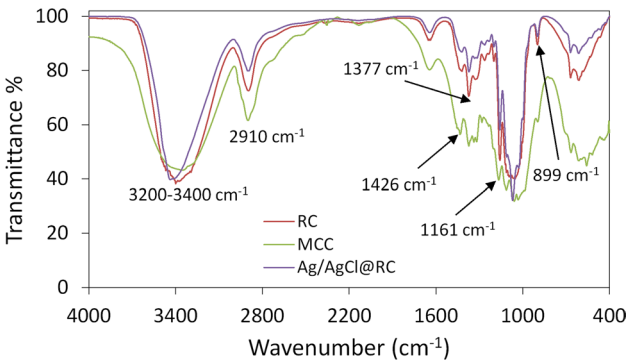

Fig. 4 FT-IR spectra of MCC, Ag/AgCl@RC, and RC films

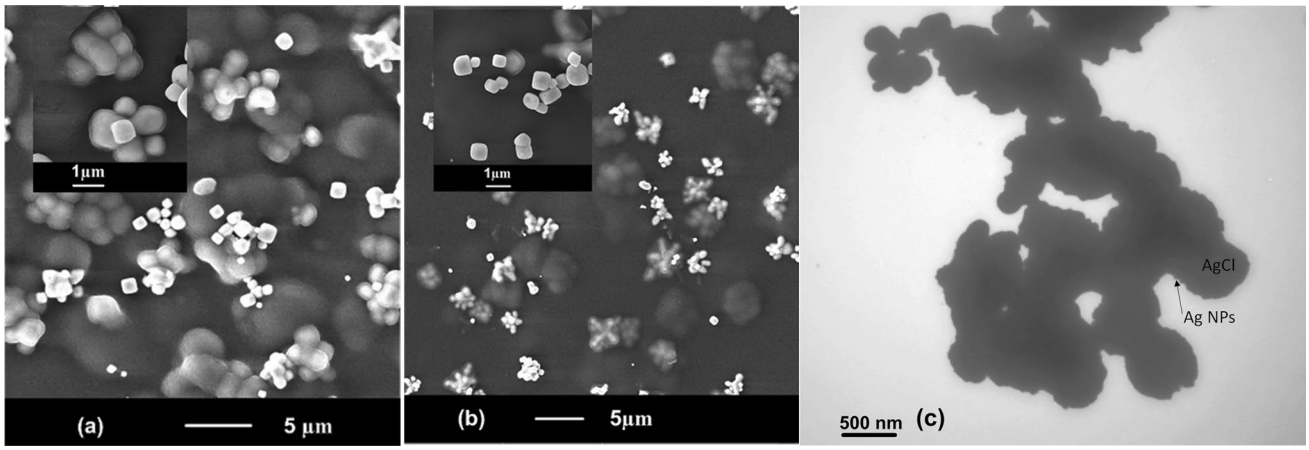

Fig. 5 SEM images of Ag/AgCl@RC-40 (**a**); Ag/AgCl@RC-20 (**b**); and TEM image of Ag/AgCl particles (**c**)

of the hybrid of silver/silver chloride within the cellulose matrix.

FT-IR spectra of the Ag/AgCl@RC and RC films

FT-IR spectra of MCC, Ag/AgCl@RC, and RC films are shown in Fig. 4. The wide band in the 3200–3400 cm^{-1} is related to O–H stretching vibrations. This band is sharper in the both Ag/AgCl@RC and RC films compared to MCC and indicates an increase in molecular hydrogen bonds in the films due to conversion of cellulose I to II (Langan et al. 1999). This structural conversion change is more supported with observation of a small red shift in the bending vibration of OH at 1161 cm^{-1}.

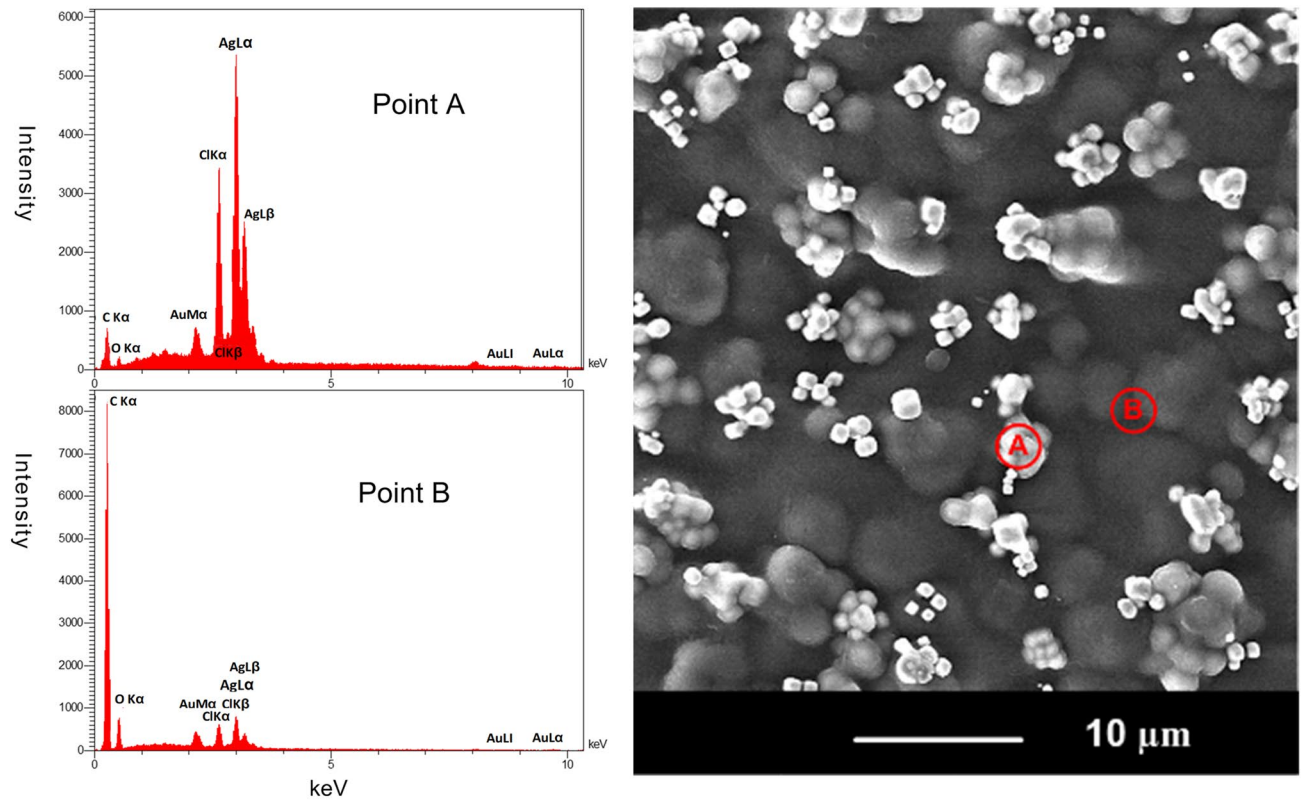

Fig. 6 SEM image of Ag/AgCl@RC-40 nanocomposite and corresponding EDS

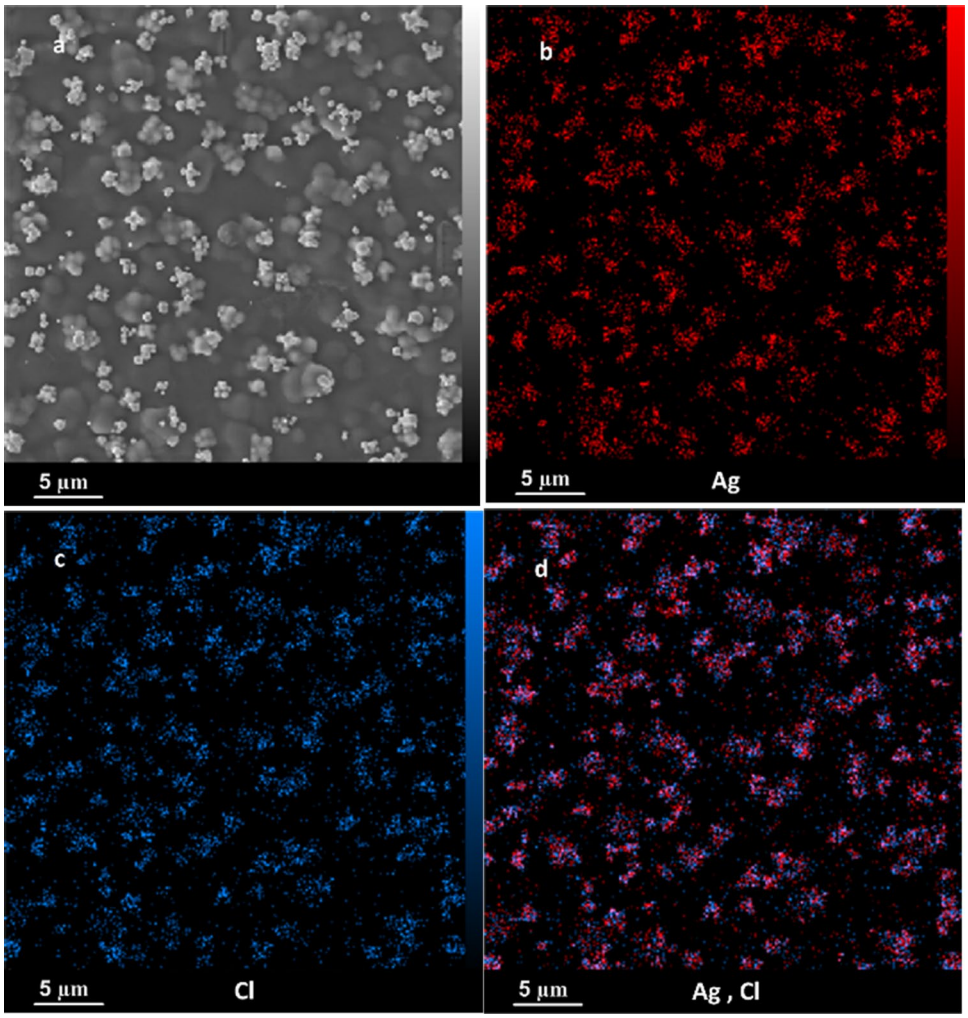

Fig. 7 SEM image of Ag/AgCl@RC-40 (**a**); EDS elemental mapping of Ag (**b**), Cl (**c**), and Ag/Cl overlay (**d**)

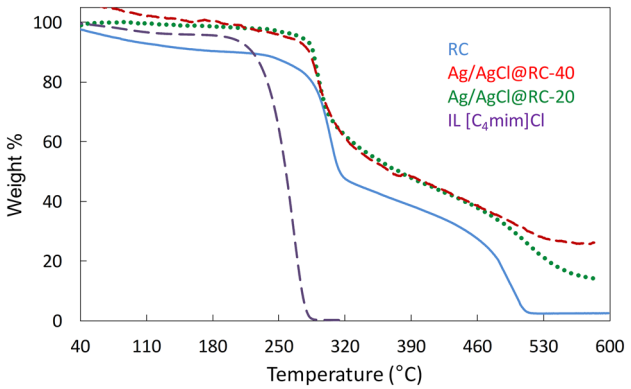

Fig. 8 Thermal stability of Ag/AgCl@RC films, RC, and IL [C_4mim]Cl under air atmosphere

A decrease in intensity of stretching vibration of C–H at 2910 cm^{-1} is probably because of angle distortion in glycosidic linkages in regenerated cellulose films. The band at 1426 cm^{-1} is related to symmetric bending vibration of CH_2, which is characteristic of crystallinity of cellulose (Synytsya and Novak 2014). The lower intensity of this band in RC and nanocomposite films compared with MCC is due to decrease in the crystalline structure of cellulose in the films. The peak at 1377 cm^{-1} is assigned to the stretching vibration of CO. The peak at 899 cm^{-1} is related to COC stretching of glycosidic units and characteristic of amorphous structure of cellulose (Synytsya and Novak 2014).

Morphology and elemental analysis of the Ag/AgCl@RC films

Figure 5 shows the SEM images of Ag/AgCl@RC nanocomposites. As seen in Fig. 5, the AgCl particles have cubic morphology and silver chloride particles anchored on the surface of cellulose and embedded within the cellulose matrix as well. There is a thin cellulosic layer surrounding the AgCl particles agglomerate encapsulated within the cellulose matrix (Fig. 5a–b). SEM images of Ag/AgCl@RC nanocomposites and TEM image of Ag/AgCl particles (Fig. 5c) show that the surface of the cubic particles is not smooth due to the formation of silver nanodomains on the

Table 1 TGA data including first onset decomposition temperature (Td1), second onset decomposition temperature (Td2), and the residual wt% at 150 °C (R150), 230 °C (R230), 350° (R350), and at 600 °C (R600)

Sample	T_{d1} (°C)	T_{d2} (°C)	R_{150}	R_{230}	R_{350}	R_{600}
IL [C_4mim]Cl	210	–	95.5	86.1	0	0
RC	240	436	91.2	89.3	43.3	2.3
RC-AG-20	264	438	98.6	97.5	54.5	15.2
RC-AG-40	260	437	99.1	97.2	53.6	34.7

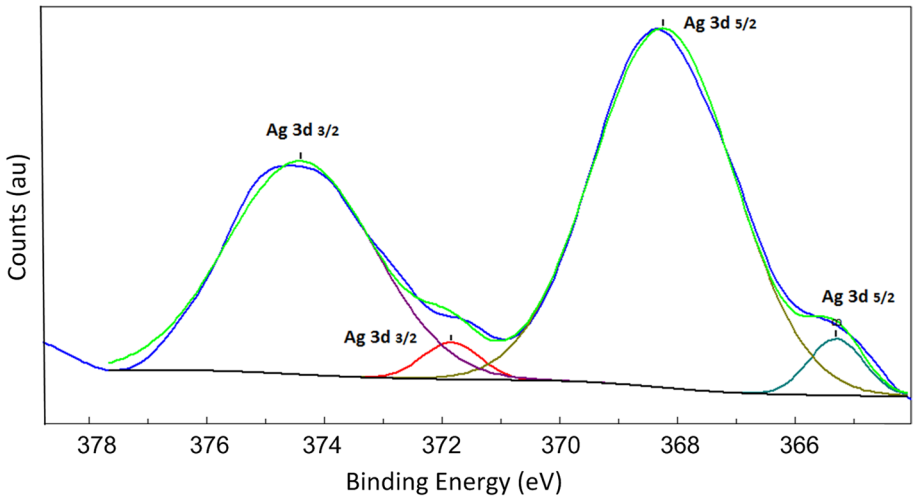

Fig. 9 The high-resolution Ag3d XPS spectrum of Ag/AgCl@RC

surface of silver chloride. A hybrid of silver/silver chloride was formed due to reducing a fraction of silver ions in silver chloride structure to Ag^0.

Elemental analysis of the Ag/AgCl@cellulose nanocomposite was carried out using energy-dispersive X-ray spectroscopy (EDS) for further confirmation of the silver chloride particle formation within the cellulose matrix (Fig. 6). The EDS results confirm the existence of silver and chloride in the cellulose matrix. Oxygen and carbon originate from the cellulose matrix, while the elements of silver and chlorine are related to Ag/AgCl in the composite. As seen in the EDS results, carbon intensity is higher in the area of B in which Ag/AgCl particles embedded within the cellulose matrix and coated with cellulose layers.

Figure 7 shows elemental mappings of Ag and Cl components and their overlay in the films. As seen in the mapping micrograph, Ag is uniformly distributed in the cellulose matrix and Cl is present in the same location with silver.

Thermal stability of the Ag/AgCl@RC films

To study the thermal stability of cellulose films, thermal weight analysis was performed on the nanocomposite of Ag/AgCl@RC and RC films (Fig. 8). Cellulose polymer with a chemical decomposition between 250 and 350 °C has a moderate thermal stability (Klemm et al. 1997). First and second thermal degradation steps are due to pyrolytic fragmentation and high cross-linking of the carbon skeleton, respectively (Klemm et al. 1998). As seen in Fig. 8, the nanocomposite films similar to regenerated cellulose have two-step thermal decomposition, but thermal stability of nanocomposite is more than cellulose. First onset degradation temperature in the RC sample starts at 240 °C, while it is about 260 °C for nanocomposites. A small weight loss is observed for RC cellulose film at temperature of 150 °C due to thermal decomposition of the residual water in the sample. But there is no weight loss in Ag/AgCl@RC films at this temperature which indicates there is no moisture in the Ag/AgCl cellulose films.

Decomposition temperatures and residual weight loss at several temperatures are shown in Table 1. Char yield of nanocomposites at temperature of 600 °C is 34.7 and 15.2% for the Ag/AgCl@RC-20 and Ag/AgCl@RC-40, respectively, while its amount is 2.3% for RC. The residual of undecomposed material at this temperature is related to Ag/AgCl in the nanocomposite films. Therefore mass content of AgCl particles in Ag/AgCl@RC-20 and Ag/AgCl@RC-40 is equal to 15.2 and 34.7%, respectively.

XPS analysis of the Ag/AgCl@RC nanocomposite

The XPS analysis was carried out to confirm the chemical state of silver on the surface of Ag/AgCl@RC

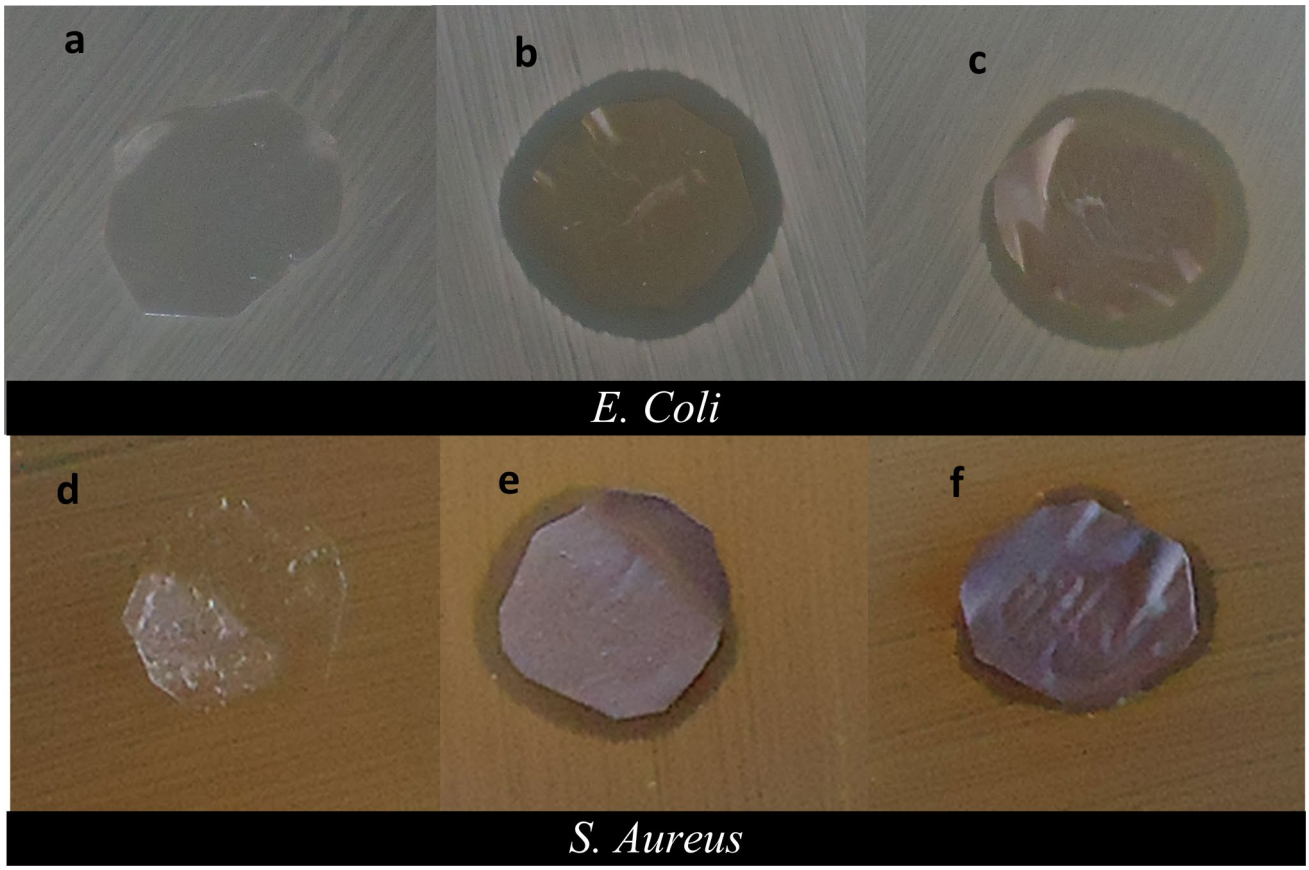

Fig. 10 Antibacterial effect against *E. Coli*: RC (**a**), Ag/AgCl@RC-20 (**b**), and Ag/AgCl@RC-40 (**c**); *S. Aureus*: RC (**d**), Ag/AgCl@RC-20 (**e**), and Ag/AgCl@RC-40 (**f**)

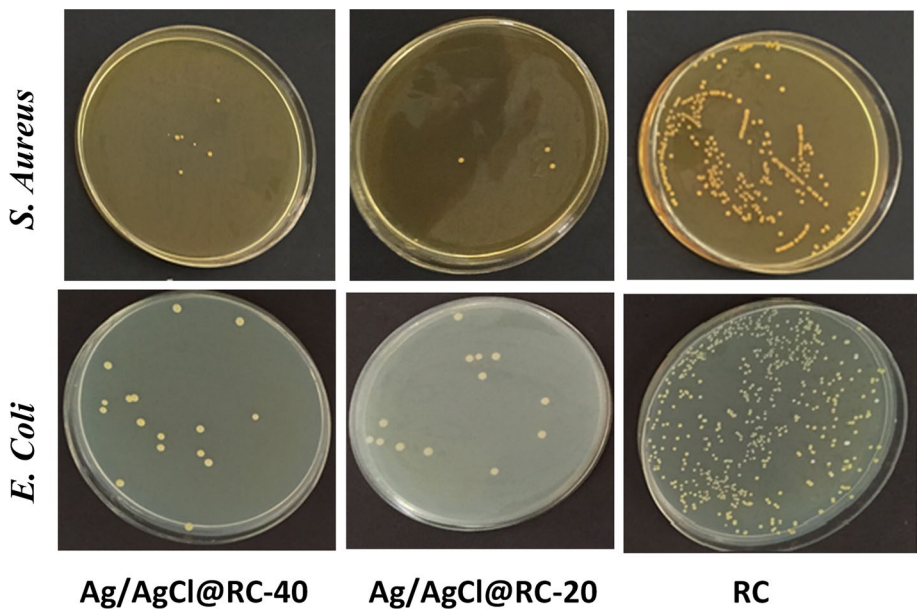

Fig. 11 Photograph of antibacterial properties of the RC, Ag/AgCl@RC-20, and Ag/AgCl@RC-40 by CFU method

nanocomposite (Fig. 9). The high-resolution Ag3d XPS spectrum of Ag/AgCl@RC shows two individual peaks at 374.4 and 368.2 eV, which is assigned to Ag 3d3/2 and Ag 3d5/2 binding energies, respectively (Jiang and Zhang 2011). The Ag 3d3/2 and Ag 3d5/2 peaks are further divided into two different small peaks at 371.8 and 365.3 eV, respectively. The peaks at 368.2 and 374.4 eV are assigned to metallic Ag, but the small peaks are related to Ag (I) in AgCl binding energies (Xu et al. 2011; Dong et al. 2012; Liu et al. 2012). The XPS results indicate the conversion of a fraction of Ag ions in silver chloride structure to their metallic state and formation of a hybrid of silver/silver chloride.

Antibacterial activity of the Ag/AgCl@RC nanocomposites

Antibacterial activity of Ag/AgCl@RC films against *E. Coli* and *S. Aureus* was qualitatively estimated by the disc diffusion method measuring the inhibition zone around the films after 24-h incubation (Fig. 10). As seen in Fig. 10, there is no inhibition zone against both bacteria for the RC control sample, indicating cellulose film has no antibacterial activity. But the growth of *E. Coli* and *S. Aureus* is inhibited in contact with the Ag/AgCl@RC nanocomposites. The inhibition zones for *E. Coli* and *S. Aureus* in the nanocomposites films were 13 and 12 mm in Ag/AgCl@RC-20 and 12.2 and 11 mm in Ag/AgCl@RC-40 film, respectively (Fig. 10). The antibacterial property of the Ag/AgCl@RC nanocomposite films was also quantitatively evaluated by CFU method (Fig. 11). The results showed the antibacterial ability of the Ag/AgCl@RC-20 and Ag/AgCl@RC-40 nanocomposites against both bacteria is about 98% and 97%, respectively.

In this study, the size of AgCl particles increased with the increase in silver content in the films. The mean size of AgCl particles in the samples of Ag/ AgCl@RC-20 (15.2% mass content) and Ag/AgCl@RC-40 (34.7% mass content) was 400 and 800 nm, respectively. Therefore, nearly similar antibacterial activity against *S. Aureus* and *E. Coli* for both samples may result from the synergistic effects of the size and mass content of silver. The results show the Ag/AgCl@RC nanocomposites have good antibacterial activity against bacterial strains of *E. Coli* and *S. Aureus*.

Conclusion

In summary, silver/silver chloride cellulose nanocomposites with antibacterial properties were synthesized through a one-step microwave method using ([C_4mim]Cl ionic liquid. The ionic liquid acts as a solvent for dissolution of cellulose and serves as a chlorine source for synthesis of silver chloride in the cellulose matrix. Silver chloride particles are anchored on the surface as well as embedded within the cellulose matrix. The cellulose-silver/silver chloride nanocomposites had potent antibacterial activity against *E. Coli* and *S. Aureus* bacteria.

Acknowledgements The authors would like to thank the financial support from Iran National Science Foundation (INSF) (Grant Number: 92013830).

Declarations

Conflict of interest The authors declare no conflict of interest.

References

Abdelhameed RM, El-Sayed HA, El-Shahat M, El-Sayed AA, Darwesh OM (2018) Novel triazolothiadiazole and triazolothiadiazine derivatives containing pyridine moiety: design, synthesis, bactericidal and fungicidal activities. Curr Bioact Compd 14(2):169–179

Abdelhameed RM, Darwesh OM, Rocha J (2019) Silva AMS (2019) IRMOF-3 biological activity enhancement by post-synthetic modification. Eur J Inorg Chem 9:1243–1249

Abdel-Monem RA, Khalil AM, Darwesh OM, Hashim AI, Rabie ST (2020) Antibacterial properties of carboxymethyl chitosan Schiff-base nanocomposites loaded with silver nanoparticles. J Macromol Sci A Pure Appl Chem 57:145–155

Ahmed H, Khattab TA, Mashaly HM, El-Halwagy AA, Rehan M (2020) Plasma activation toward multi-stimuli responsive cotton fabric via in situ development of polyaniline derivatives and silver nanoparticles. Cellulose 27(5):2913–2926

Alahmadi NS, Betts JW, Heinze T, Kelly SM, Koschella A, Wadhawan JD (2018) Synthesis and antimicrobial effects of highly dispersed, cellulose-stabilized silver/cellulose nanocomposites. RSC Adv 8:3646–3656

Alavi M, Rai M (2019) Recent progress in nanoformulations of silver nanoparticles with cellulose, chitosan, and alginic acid biopolymers for antibacterial applications. Appl Microbiol Biotechnol 103:8669–8676

Atta AM (2021) Immobilization of silver and strontium oxide aluminate nanoparticles integrated into plasma-activated cotton fabric: luminescence, superhydrophobicity, and antimicrobial activity. Luminescence 36(4):1078–1088

Atta AM, Abomelka HM (2021) Multifunctional finishing of cotton fibers using silver nanoparticles via microwave-assisted reduction of silver alkylcarbamate. Mater Chem Phys 260:124137

Bagheri M, Rabieh S (2013) Preparation and characterization of cellulose-ZnO nanocomposite based on ionic liquid ([C_4mim]Cl). Cellulose 20:699–705

Chen H, Xiao L, Huang J (2014) Template synthesis of Ag/AgCl microrods and their efficient visible light-driven photocatalytic performance. Mater Res Bulletin 57:35–40

Cheng F, Betts JW, Kelly SM, Hector AL (2015) Green synthesis of highly concentrated aqueous colloidal solutions of large starch-stabilised silver nanoplatelets. Mater Sci Eng C 46:530–537

Choi M, Shin KH, Jang J (2010) Plasmonic photocatalytic system using silver chloride/silver nanostructures under visible light. J Colloid Interface Sci 341:83–87

Dai L, Liu R, Hu LQ, S, CL, (2017) Simple and green fabrication of AgCl/Ag-cellulose paper with antibacterial and photocatalytic activity. Carbohyd Polym 174:450–455

Darwesh OM, Matter IA, Eida MF, Moawad H, Oh YK (2019) Influence of nitrogen source and growth phase on extracellular biosynthesis of silver nanoparticles using cultural filtrates of scenedesmus obliquus. Appl Sci 9(7):1465

Dong L, Liang D, Gong R (2012) In Situ photoactivated AgCl/Ag nanocomposites with enhanced visible light photocatalytic and antibacterial activity. Eur J Inorg Chem 2012:3200–3208

Dong YY, He J, Sun SL, Ma MG, Fu LH, Sun RC (2013) Environmentally friendly microwave ionic liquids synthesis of hybrids from cellulose and AgX (X = Cl, Br). Carbohyd Polym 98:168–173

Dong YY, Deng F, Zhao JJ, He J, M, MG, Xu F, Sun RC, (2014) Environmentally friendly ultrasound synthesis and antibacterial activity of cellulose/Ag/AgCl hybrids. Carbohyd Polym 99:166–172

El-Naggar ME, Khattab TA, Abdelrahman MS, Aldalbahi A, Hatshan MF (2021) Development of antimicrobial, UV blocked and photocatalytic self-cleanable cotton fibers decorated with silver nanoparticles using silver carbamate and plasma activation. Cellulose 28:1105–1121

Franz G, Blaschek W (1990) Cellulose. In Methods in plant biochemistry Carbohydrates, vol 2 (ed. PM Dey), Academic Press, London, pp 291–322

Gudimalla A, Jose J, Rajendran JV, Gurram G, Thomas S (2022) Synthesis of silver nanoparticles by plant extract, incorporated into alginate films and their characterizations. Chem Pap 76:1031–1043

Islam S, Butola BS, Gupta A, Roy A (2019) Multifunctional finishing of cellulosic fabric via facile, rapid in-situ green synthesis of AgNPs using pomegranate peel extract biomolecules. Sustain Chem Pharm 12:100135

Jiang J, Zhang LZ (2011) Rapid microwave-assisted nonaqueous synthesis and growth mechanism of AgCl/Ag, and its daylight-driven plasmonic photocatalysis. Chem Eur J 17:3710–3717

Katouah H, El-Metwaly NM (2021) Plasma treatment toward electrically conductive and superhydrophobic cotton fibers by in situ preparation of polypyrrole and silver nanoparticles. React Funct Polym 159:104810

Klemm D, Heinz T, Philipp B, Wegenknecht W (1997) New approaches to advanced polymers by selective cellulose functionalization. Acta Polym 48:277–297

Klemm D, Philipp B, Heinz T, Wegenknecht W (1998) Comprehensive cellulose chemistry,vol 1: fundamentals and analytical methods. Wiley-VCH, Weinheim

Koide M, Wataoka I, Urakawa H, Kajiwara K, Henniges U, Rosenau T (2019) Intrinsic characteristics of cellulose dissolved in an ionic liquid: the shape of a single cellulose molecule in solution. Cellulose 26:2233–2242

Kontturi E, Tammelin T, Osterberg M (2006) Cellulose-model films and the fundamental approach. Chem Soc Rev 35:1287–1304

Kucekova Z, Kasparkova V, Humpolicek P, Sevcikova P, Stejskal J (2013) Antibacterial properties of polyaniline-silver films. Chem Pap 67:1103–1108

Kumar VA, Nakajima Y, Uchida T, Hanajiri T, Maekawa T (2016) Synthesis of nanoparticles composed of silver and silver chloride for a plasmonic photocatalyst using an extract from needles of Pinus densiflora. Mater Lett 176:169–172

Kumar SSD, Rajendran NK, Houreld NN, Abrahamse H (2018) Recent advances on silver nanoparticle and biopolymer based biomaterials for wound healing applications. Int J Biol Macromol 115:165–175

Lal SS, Mhaske ST (2018) AgBr and AgCl nanoparticle doped TEMPO-oxidized microfiber cellulose as a starting material for antimicrobial filter. Carbohyd Polym 191:266–279

Langan P, Nishiyama Y, Chanzy H (1999) A revised structure and hydrogen-bonding system in cellulose II from a neutron fiber diffraction analysis. J Am Chem Soc 121:9940–9946

Langan P, Sukumar N, Nishiyama Y, Chanzy H (2005) Synchrotron X-ray structures of cellulose Iβ and regenerated cellulose II at ambient temperature and 100 K. Cellulose 12:551–562

Liu C, Yang D, Wang Y, Shi J, Jiang Z (2012) Fabrication of antimicrobial bacterial cellulose–Ag/AgCl nanocomposite using bacteria as versatile biofactory. J Nanopart Res 14:1084–1092

Liu X, Chang PR, Zheng P, Anderson DP, Ma X (2015) Porous cellulose facilitated by ionic liquid [BMIM]Cl: fabrication, characterization, and modification. Cellulose 22:709–715

Ma Z, Yin M, Qi Z, Ren X (2018) Preparation of durable antibacterial cellulose with AgCl nanoparticles. Fiber Polym 19:2097–2102

Peng X, Wang S, Zhang X, Shu Y, Su S, Zhu J (2017) Ag@AgCl embedded on cellulose film: a stable, highly efficient and easily recyclable photocatalyst. Cellulose 24:4683–4689

Qi H (2017) Novel functional materials based on cellulose. Springer International Publishing, Verlag

Rehan M, Nada AM, Khatta TA, Abdelwahed NAM, El-Kheirf AAA (2020) Development of multifunctional polyacrylonitrile/silver nanocomposite films: antimicrobial activity, catalytic activity, electrical conductivity, UV protection and SERS-active sensor. J Mater Res Technol 9(4):9380–9394

Sarac AS (2016) Nanofibers of Conjugated Polymers. 1st edn. Jenny Stanford Publishing.

Sayyed AJ, Deshmukh NA, Pinjari DV (2019) A critical review of manufacturing processes used in regenerated cellulosic fibres: viscose, cellulose acetate, cuprammonium, LiCl/DMAc, ionic liquids, and NMMO based lyocell. Cellulose 26:2913–2940

Shu Y, Lv J, Peng X, Zhang X, Su S, Zhu J (2018) In situ controllable synthesis of Ag@AgCl in cellulose film and its effect on antifouling properties. Cellulose 25:5175–5184

Silva RD, Vongsanga K, Wang X, Byrne N (2015) Cellulose regeneration in ionic liquids: factors controlling the degree of polymerization. Cellulose 22:2845–2849

Song J, Roh J, Lee I, Jang J (2013) Low temperature aqueous phase synthesis of silver/silver chloride plasmonic nanoparticles as visible light photocatalysts. Dalton Trans 42:13897–13904

Stejskal J, Trchová M, Kovářová J, Prokeš J, Omastová M (2008) Polyaniline-coated cellulose fibers decorated with silver nanoparticles. Chem Pap 62:181–186

Stevanovic T (2018) Chemistry of lignocellulosics: current trends. 1st edn. CRC Press.

Swatloski RP, Spear SK, Holbrey JD, Rogers RD (2002) Dissolution of cellulose with ionic liquids. J Am Chem Soc 124:4974–4975

Synytsya A, Novak M (2014) Structural analysis of glucans. Ann Transl Med 2(2):17

Tang L, Tang F, Li M, Li L (2018) Facile synthesis of Ag@AgCl-contained cellulose hydrogels and their application. Colloids Surf A Physicochem Eng Asp 553:618–623

Trinh ND, Nguyen TTB, Nguyen TH (2015) Preparation and characterization of silver chloride nanoparticles as an antibacterial agent. Adv Nat Sci Nanosci Nanotechnol 6:045011

Vekariya RL (2017) A review of ionic liquids: applications towards catalytic organic transformations. J Mol Liq 227:44–60

Verma C, Mishra A, Chauhan S, Verma P, Srivastava V, Quraish MA, Ebenso EE (2019) Dissolution of cellulose in ionic liquids and their mixed cosolvents: a review. Sustain Chem Pharm 13:100162

Vosmanská V, Kolářová K, Rimpelová S, Kolská Z, Švorčík V (2015) Antibacterial wound dressing: plasma treatment effect on chitosan impregnation and in situ synthesis of silver chloride on cellulose surface. RSC Adv 5:17690–17699

Wang S, Luo T, Zhu J, Zhang X, Su S (2016) A facile way to fabricate cellulose-Ag@AgCl composites with photocatalytic properties. Cellulose 23:3737–3745

Wang S, Zhang X, Luo T, Zhu J, Su S (2017) Preparation of native cellulose-AgCl fiber with antimicrobial activity through one-step electrospinning. J Biomater Sci Polym Ed 28:284–292

Xu H, Li H, Xia J, Yin S, Luo S, Liu L, Xu L (2011) One-pot synthesis of visible-light-driven plasmonic photocatalyst Ag/AgCl in ionic liquid. ACS Appl Mater Interfaces 3:22–29

Zhang J, Wu J, Yu J, Zhang X, He J, Zhang J (2017) Application of ionic liquids for dissolving cellulose and fabricating cellulose-based materials: state of the art and future trends. Mater Chem Front 1:1273–1290

Zhang X, Shu Y, Su S, Zhu J (2018) One-step coagulation to construct durable anti-fouling and antibacterial cellulose film exploiting Ag@AgCl nanoparticle-triggered photo-catalytic degradation. Carbohyd Polym 181:499–505

Zhao X, Zhang J, Wang B, Zada A, Humayun M (2015) Biochemical synthesis of Ag/AgCl nanoparticles for visible-light-driven photocatalytic removal of colored dyes. Materials 8:2043–2053

Zhou Z, Peng X, Zhong L, Wu L, Cao X, Sun RC (2016) Electrospun cellulose acetate supported Ag@AgCl composites with facet-dependent photocatalytic properties on degradation of organic dyes under visible-light irradiation. Carbohydr Polym 136:322–328